Available online at www.sciencedirect.com
ScienceDirect
Trans. Nonferrous Met. Soc. China 34(2024) 1487−1495
Transactions of Nonferrous Metals Society of China
www.tnmsc.cn

Microstructure of corrosion product film formed on aged WE43 alloy

Yong CAI[1,2], Yi-peng CHEN[1,2], Hong YAN[2,3], Rong-shi CHEN[2]

1. School of Materials Science and Engineering, University of Science and Technology of China, Shenyang 110016, China;
2. Shi-changxu Innovation Center for Advanced Materials, Institute of Metal Research, Chinese Academy of Sciences, Shenyang 110016, China;
3. School of Materials Science and Engineering, Shandong University of Science and Technology, Qingdao, Shandong 266590, China

Received 10 November 2022; accepted 29 March 2023

Abstract: A dense three-layer corrosion product film was formed on aged WE43 alloy in 3.5 wt.% NaCl solution. The microstructure of the film was analyzed in detail by TEM. The three-layer corrosion product film is composed of RE_2O_3, MgO layer doped with RE_2O_3 and $Mg(OH)_2$ layer doped with RE_2O_3 from the inside to the outside. A large amount of rare earth oxide particles formed both by the outward oxidation of rare earth precipitates and rare earth elements, are the main reason for the formation of the corrosion film. The RE_2O_3 has the preferential orientation with $(\bar{2}11)$ plane and [231] direction parallel to (002) plane and $[\bar{1}\bar{1}0]$ direction of MgO, respectively. Thus, the rare earth oxide particles can fill the gap of porous MgO layer, and improve the compactness of the film. The inner RE_2O_3 layer and mixed layer of MgO and RE_2O_3 play an important role in the formation of the film. The compact inner film can prevent the corrosion medium from reacting with the Mg matrix.

Key words: magnesium alloy; corrosion product film; HRTEM; precipitate; oxidation

1 Introduction

Magnesium alloys are promising structural materials in transportation and aerospace industries because of their properties of high specific strength and high specific stiffness [1,2]. In addition, magnesium is a beneficial element that does not disrupt metabolic processes, making it suitable for body implants [3]. Since magnesium alloys are chemically active and have a high affinity for oxygen, the relatively poor corrosion resistance is an important issue preventing the widespread application. The corrosion resistance of magnesium alloys is governed by alloying elements, microstructure and corrosion film [4−6]. A lot of fundamental corrosion investigations in the past decade have involved the surface film formed on pure magnesium and magnesium alloys. For pure magnesium, the corrosion film has a bi-layered structure composed of $Mg(OH)_2$ outer layer and MgO inner layer [7−9]. TAHERI et al [10] further revealed that the surface film of pure magnesium is a diffuse bi-layer structure, and the $Mg(OH)_2$-rich outer layer is relatively thick (~700 nm) and less porous while the nano-crystalline MgO-rich inner layer is much thinner (50−90 nm) and more porous by the transmission electron microscope (TEM). For magnesium alloys, the surface film has similar bi-layered structure [9,11,12]. However, there is no enrichment of alloy elements in the film for AZ series magnesium alloys [13,14], while rare earth

Corresponding author: Hong YAN, Tel: +86-24-23915897, Fax: +86-24-23894149, E-mail: yanhong5871@163.com;
Rong-shi CHEN, Tel: +86-24-23926646, Fax: +86-24-23894149, E-mail: rschen@imr.ac.cn

DOI: 10.1016/S1003-6326(24)66485-X

elements are found to incorporate into the film from the matrix in rare earth containing magnesium alloys [5]. It is interesting to note that even if the alloying elements are present inside the corrosion film, the film structure does not change significantly compared with the film in pure magnesium immersed in NaCl solution [5]. We reported that the corrosion rate of aged WE43 alloy was lower than that of solid solution treatment (T4) condition in 3.5 wt.% NaCl solution, and this is caused by the interaction between finely dispersed precipitates and the inward growth of corrosion reaction. CHU and MARQUIS [5] pointed out that the precipitated phases did not undergo anodic dissolution, but only hindered the channel of the corrosive medium into the magnesium matrix. However, LIU et al [15] demonstrated that for the Y-containing precipitates, anodic dissolution preferentially occurred, which led to the formation of Y-containing corrosion film. Therefore, it is controversial whether the anodic dissolution of rare earth precipitates promotes the formation of corrosion product film in the corrosion behavior of magnesium alloys during internal oxidation, which needs further experimental demonstration.

Among all rare earth magnesium alloys, WE43 alloy maintains excellent mechanical properties and heat resistance [16], which is a very successful commercial rare earth magnesium alloy [17]. Up to now, a large number of studies have reported the immersion corrosion behavior of WE43 alloy [18−22]. Most of the previous studies discussed the corrosion behavior of WE43 alloy under different experimental conditions. However, the direct imaging of the surface film on the cross-section is absent, especially the detailed characterization of corrosion film. Thus, analyzing the corrosion film formed on aged WE43 alloy in 3.5 wt.% NaCl solution was carried out in this work, in order to elucidate the formation process of the corrosion product film and reveal the role of the precipitates in the film.

2 Experimental

The chemical composition of WE43 alloy in this work was determined to be Mg−3.71Y−1.35Gd−2.08Nd−0.58Zr (wt.%) by the inductively coupled plasma−atomic emission spectrometry (ICP−AES). After milling, rectangular WE43 plates (50 mm in length, 30 mm in width and 5 mm in thickness) were yielded and treated by solid solution (T4: alloy solution treatment for 8 h at 525 °C), followed by aging treatment (T6: aging for 16 h at 250 °C) [23]. All specimens were ground using 400#, 800#, 1200#, 2000#, 3000#, and 5000# SiC sandpapers. Then, the surface was mechanically polished with 1.0 μm diamond polishing paste and ultrasonically cleaned with anhydrous ethanol. The local alternating current impedance (LEIS) was measured in the microscopic electrochemical test in order to prove preferential anodic dissolution of the precipitates. The LEIS test area was 30 μm × 30 μm and the test solution was that the neutral 3.5 wt.% NaCl aqueous solution was diluted 1000 times with deionized water, that is, the solution concentration was 0.0035 wt.% NaCl, in order to slow down the corrosion process and provide sufficient time for LEIS detection. The parameters for measuring the LEIS were scanning speed of 1 μm/s, test frequency of 10−0.1 Hz and AC signal of 20 mV. The samples were immersed in 3.5 wt.% NaCl solution for 24 h to obtain corrosion film for further microstructure observation.

The microstructure of the cross-sectional morphologies was determined by a JEM−2100F transmission electron microscope (TEM). The aged sample after immersing in the neutral 3.5 wt.% NaCl aqueous solution with pH value of 7 for 24 h was fabricated to semi-circles of *d*3 mm × 0.5 mm by wire cutting. The sample edge with oxide film was glued together into a complete *d*3 mm × 0.5 mm wafer. The copper ring was pasted on the wafer with an outer diameter of 3 mm, an inner diameter of 1.5 mm, and a thickness of 30 μm. The wafer stuck together by glue was easily separated into two halves during grinding process. The copper ring can be fixed to the wafer without being separated into two halves. The wafer was ground successively with SiC sandpapers until the thickness of the sample was 30 μm. A Gatan 691 ion beam thinning apparatus was used to obtain the thin area needed for JEM−2100F TEM experiment.

3 Results

Figures 1(a, b) show the cross-sectional SEM morphologies of the corrosion product film of the solutionized and aged WE43 alloys, respectively. Compared with the solutionized alloy, the layer of

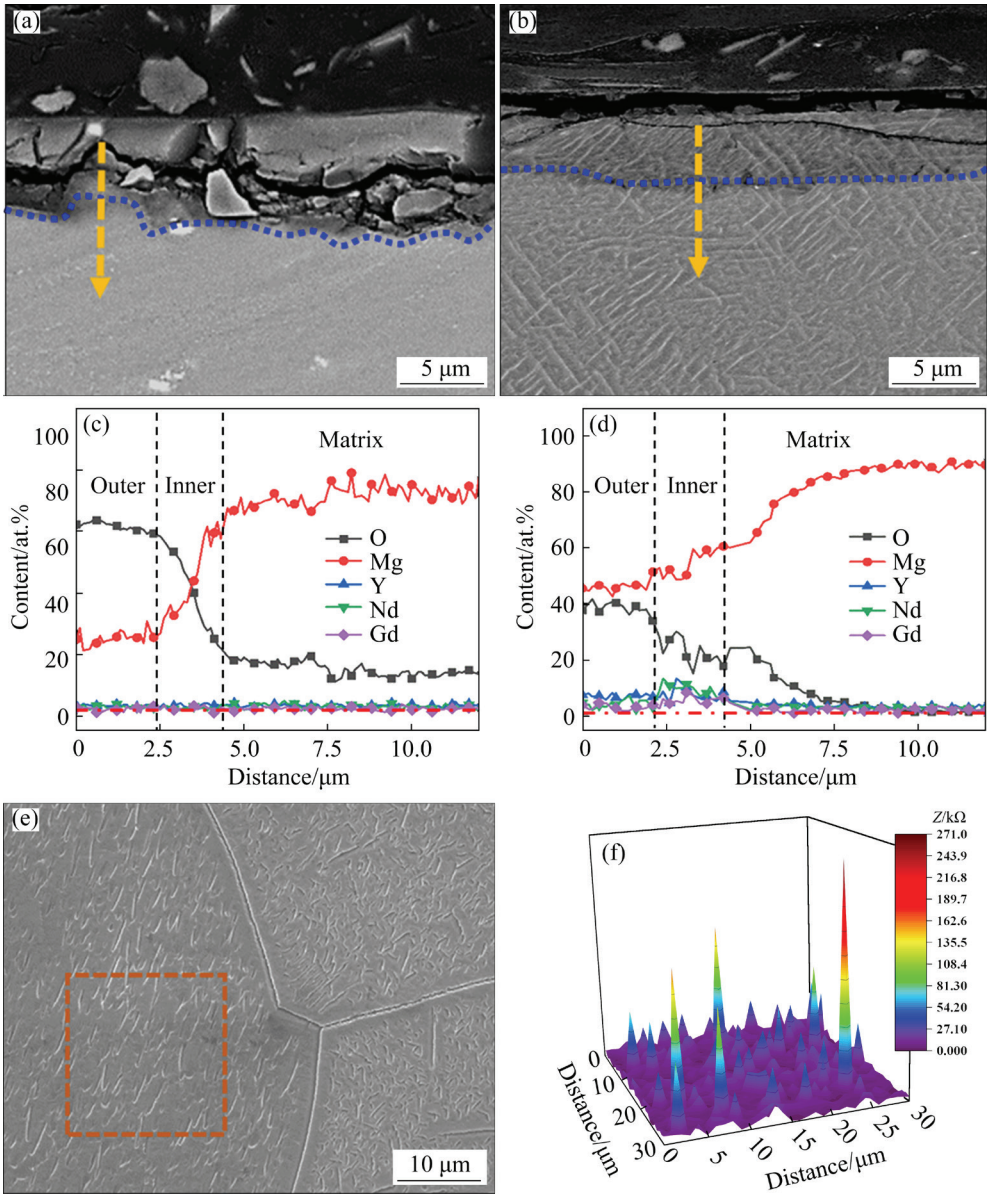

Fig. 1 Cross-sectional SEM morphologies (a, b) and EDS compositional profiles (c, d) of corrosion film of solutionized (a, c) and aged (b, d) WE43 alloys, morphology of sample for LEIS test (e) (The orange dotted box represents the test area of aged WE43 alloy), and LEIS local impedance spectrum (f) of test area in (e)

the aged alloy is much more compact and the thickness is reduced by about half. The aged alloy exhibits better corrosion resistance. The EDS line scanning is conducted to investigate the composition evolution of the corrosion product film along depth direction. As shown in Fig. 1(c), for the solutionized alloy, the content of O and Mg is 61.5 at.% and 29.8 at.% in the outer layer and 41.5 at.% and 40.4 at.% in the inner layer, respectively. The O/Mg molar ratio is about 2:1 in the outer layer and 1:1 in the inner layer. By comparing the EDS line scanning results of the corrosion film of the solutionized WE43 alloy in 3.5 wt.% NaCl solution by CHU and MARQUIS [5], it can be determined that the film in this work is also divided into two layers: thick outer layer $Mg(OH)_2$ and thin inner layer MgO. In addition, the content of rare earth elements in the film is the same as that in the matrix, indicating that no obvious outward diffusion of rare earth elements occurs during inward corrosion reaction. For the aged sample, a large number of fine dispersed precipitates appear in the corrosion film, similar to those in the matrix (Fig. 1(b)). As shown in Fig. 1(d), the content of O and Mg is 41.2 at.% and 44.6 at.% in the outer layer and 18.9 at.% and

57.8 at.% in the inner layer, respectively. The O/Mg molar ratio in the outer layer is almost equal, but the Mg atomic number in the inner layer is greater than that of O. The content of rare earth elements in the corrosion film is higher than that in the matrix, and the content in the inner layer is the highest. This may be due to the anodic dissolution of precipitates β-$Mg_{14}(Nd,Gd)_2Y$ in the film and outward oxidation of rare earth elements during corrosion process. To demonstrate that dispersed precipitates are involved in the corrosion process, LEIS is conducted to characterize the local impedance spectrum in the grain. As shown in Figs. 1(e, f), dispersed impedance peaks appear in the test area. The precipitates preferentially dissolve anodically to form rare earth oxides, resulting in an increase in local impedance values. The corrosion film in the aged alloy is much more compact than that in solutionized alloy (Figs. 1(a, b)). Therefore, it is speculated that rare earth oxides are involved in the formation of corrosion product film in the aged WE43 alloy.

TEM is used to further explore the corrosion product film structure (Fig. 2). Compared with the matrix, there are more particles in the film (Fig. 2(a)). As far as we know, the precipitates in WE43 alloy cannot be formed by atomic diffusion at room temperature, so these particles are formed through the outward oxidation of β-$Mg_{14}(Nd,Gd)_2Y$ precipitates. The EDS mappings (Figs. 2(b−f)) show the distribution of Mg, O and RE elements. The Analysis Station software is used to analyze the content of rare earth elements. The results show that the content of rare earth elements is 4.06 at.% in the corrosion product film and is 2.04 at.% in the matrix. The higher content of rare earth elements in the film is consistent with the results in Fig. 1(d). Therefore, not only the inward oxidation of Mg [5,13,24], but also the outward oxidation of rare earth elements take place in the aged alloy during oxidation process.

Figure 3(a) shows the HRTEM image of the interface between film and Mg matrix of the aged alloy. Obviously, the film contains various grain-oriented oxide nanocrystals (white dot region). The SAED pattern of the film shows the characteristics of polycrystalline diffraction rings (Fig. 3(b)), which also confirms that the film is polycrystalline. Through the calibration of the diffraction rings, it can be found that the film contains MgO and rare earth oxides (Y_2O_3, Nd_2O_3, Gd_2O_3). Figure 3(c) shows the FFT pattern and the pattern is calibrated as Mg matrix. The crystal spacing is calibrated by Digital Micrograph (DM) software. The G3 region

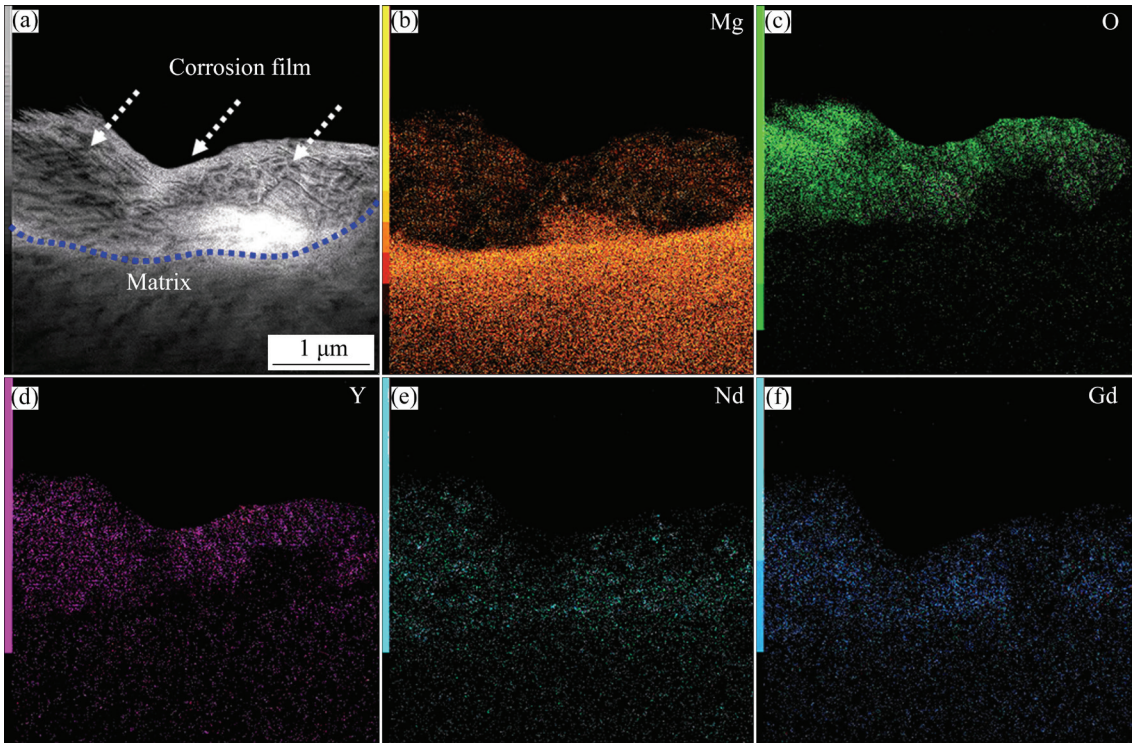

Fig. 2 Scanning transmission electron microscopy (STEM) image (a), and corresponding elemental mappings of Mg (b), O (c), Y (d), Nd (e) and Gd (f) of corrosion product film on aged WE43 alloy

in Fig. 3(a) is Mg matrix, and the G1 and G2 nanocrystals are cubic crystalline Y_2O_3 and MgO, respectively. Interestingly, these oxidized nanocrystals are embedded in the G3 matrix region, indicating the phenomena: (1) oxygen inward diffusion into the Mg matrix; (2) rare earth oxides forming at the oxidation front of the film. This also confirms from the atomic scale that the corrosion product film grows inward and the chemical activity of rare earth elements is higher than that of Mg, leading to the preferential loss of electrons and the oxidation reaction. It should be noted that more precipitates in the film in Fig. 2(a) are actually rare earth oxides doped in the film.

The doping mode of rare earth oxides in the film is further studied by HRTEM. As shown in Fig. 4(a), cubic crystalline MgO grains with different orientations are distributed around the cubic crystalline Y_2O_3 grain. As mentioned above, due to the inward growth of the layer, the growth direction of the film is from top to bottom in the HRTEM image. The region of orange dotted box

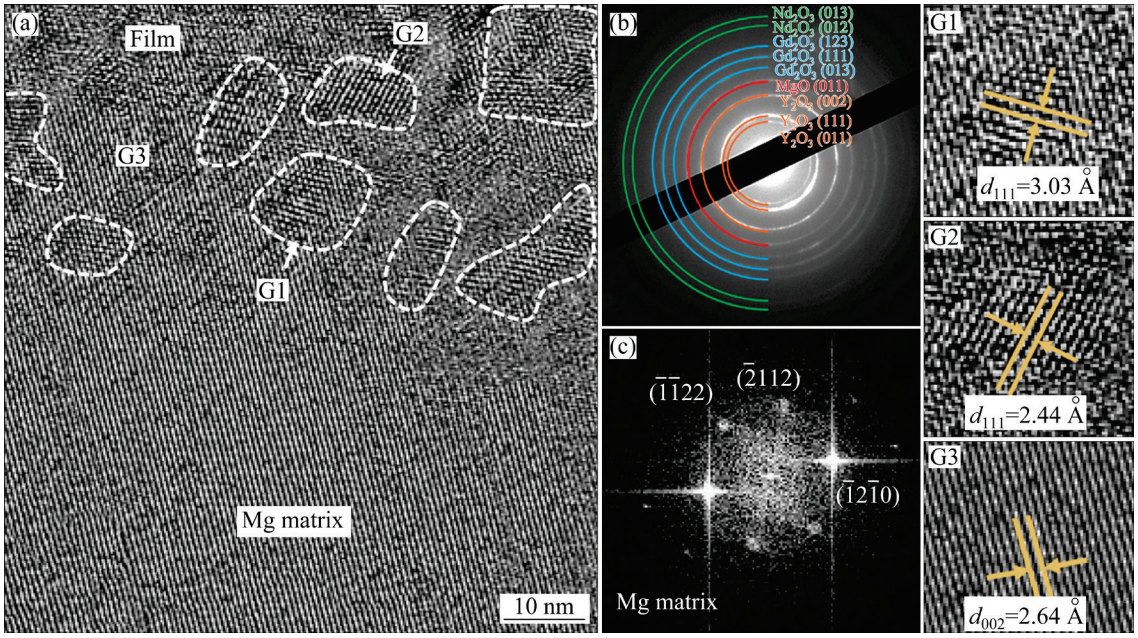

Fig. 3 High-resolution transmission electron microscopy (HRTEM) image of interface between film and Mg matrix of aged alloy: (a) Bright field image; (b) Selected area electron diffraction (SAED) pattern of corrosion product film; (c) Fast Furious transform (FFT) map of Mg matrix (G1, G2 and G3 are HRTEM images of Y_2O_3, MgO and Mg matrix, respectively)

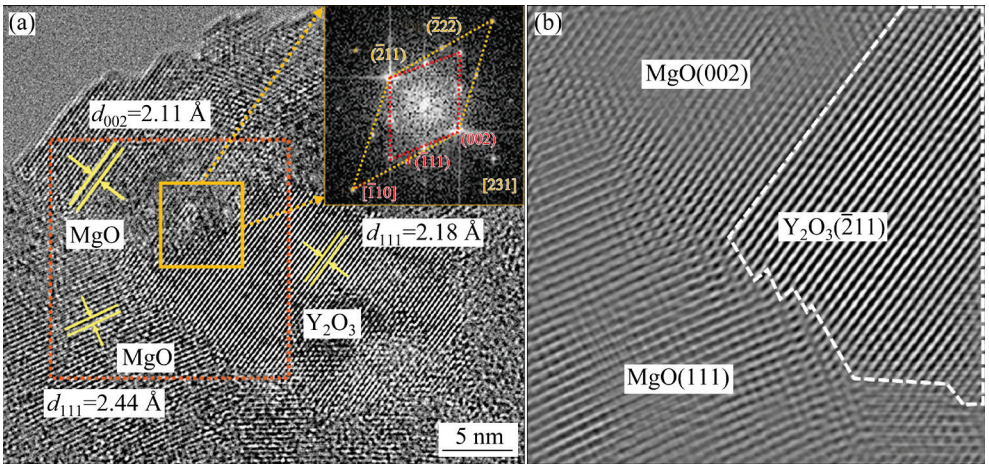

Fig. 4 HRTEM image of corrosion product film (a), and inverse fast Furious transform (IFFT) map (b) of orange dotted box in (a)

contains MgO (002), MgO (111) and Y_2O_3 ($\bar{2}11$) grains. The FFT patterns for the solid line box suggest that the Y_2O_3 has the relationship $(\bar{2}11)_{Y_2O_3}$// $(002)_{MgO}$ and $[231]_{Y_2O_3}$//$[\bar{1}\bar{1}0]_{MgO}$ with MgO. The IFFT of the dotted box region is performed by DM software (Fig. 4(b)). It shows the structural misfits accommodated by defects and distortions. The ($\bar{2}11$) plane of Y_2O_3 grows coherently along the (002) plane of MgO, showing low mismatch with MgO grains. Therefore, Y_2O_3 is prone to grow and fill the gap between MgO grains. This is the essential reason that rare earth oxides can promote the formation of corrosion product film.

4 Discussion

It is confirmed that film growth mechanism is dominated by inward transport of oxygen and hydrogen diffusion rather than by outward diffusion in Mg alloys [25]. In addition, the inner MgO layer is formed by anodic oxidation and the outer $Mg(OH)_2$ layer is formed by the hydration of the inner MgO layer [5]. Figure 5(a, b) show the schematic diagrams of the microstructure evolution and formation mechanism of the film. The Pilling−Bedworth ratio (PBR) value of Mg oxide is 0.81 [26], which could not form a dense film. TAHERI et al [10] also pointed out that the inner MgO layer in the corrosion film of pure Mg is porous. However, CHU and MARQUIS [5] observed that the inner layer is dense in the corrosion film of aged WE43 alloy by TEM, which is consistent with the observation results in this work. The inner MgO layer is related to rare earth oxides. The PBR of the oxides formed from the precipitated phases in Mg alloys was introduced in detail by JIANG et al [27]. For aged WE43 alloy, the PBR of rare earth oxides formed from the precipitate β-$Mg_{14}(Nd,Gd)_2Y$ can be calculated by

$$\mathrm{PBR}=\frac{V_{RE_2O_3}}{2V_{RE}} \tag{1}$$

where $V_{RE_2O_3}$ is the molar volume of RE_2O_3 and V_{RE} is the volume of RE atoms in $Mg_{14}(Nd,Gd)_2Y$. According to the data in Ref. [27], the molar volume of Y_2O_3, Gd_2O_3 and Nd_2O_3 is 45.0719, 48.9201 and 46.4738 cm^3/mol, respectively. Because each RE_2O_3 molecule contains two RE atoms, 2 mol RE atoms are considered in the calculation.

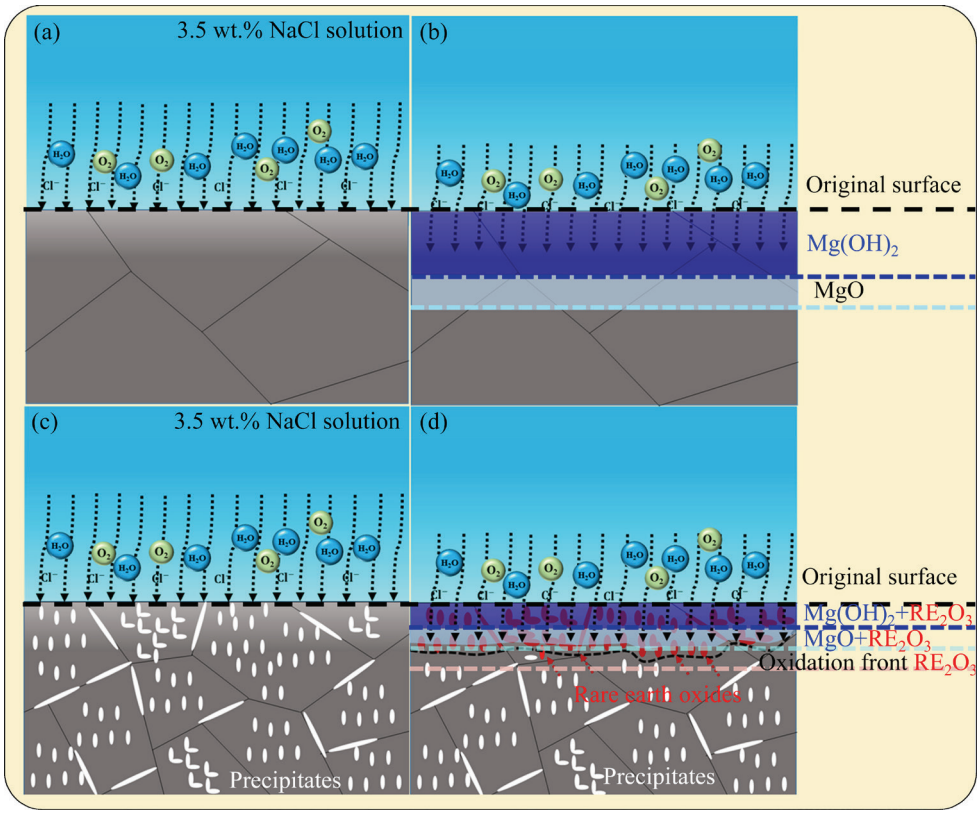

Fig. 5 Schematic diagrams of formation mechanism and microstructure of corrosion product film on WE43 alloys: (a, b) Solutionized alloy; (c, d) Aged alloy

The density of the $Mg_{14}(Nd,Gd)_2Y$ unit cell is 2.8536 g/cm^3 according to the XRD card. The molar mass of the precipitate is 730.667 g/mol. Therefore, the molar volume of $Mg_{14}(Nd,Gd)_2Y$ is calculated to be 256.0510 cm^3/mol. According to the data in Ref. [27], the molar volume of Mg is 13.9845 cm^3/mol. The two molar volumes of RE atoms in $Mg_{14}(Nd,Gd)_2Y$ unit cell are calculated via the following formula [27,28]:

$$V_{RE}=V_{precipitate}-14V_{Mg} \quad (2)$$

where $V_{precipitate}$ and V_{Mg} are the molar volumes of $Mg_{14}(Nd,Gd)_2Y$ and Mg, respectively. The molar volume of RE atoms is calculated to be 120.536 cm^3/mol. According Eq. (1), the PBR value of rare earth oxides formed from the precipitate $Mg_{14}(Nd,Gd)_2Y$ can be calculated to be 1.1653, which means that the anodic oxidation film is a compact film. Not only the inward transport of oxygen and hydrogen diffusion, but also the outward oxidation of rare earth elements to the corrosion film takes place during the inward corrosion reaction. In addition, the oxidation of fine dispersed precipitates also leads to the formation of rare earth oxides in the film. HRTEM shows that the inner layer is mainly composed of rare earth oxides and MgO, and the oxidation front is rare earth oxides, so the corrosion product film of aged WE43 alloy actually is three-layer structure. Figures 5(c, d) show the schematic diagrams of the formation mechanism and microstructure of the three-layer film. The multilayer film is composed of RE_2O_3, MgO + RE_2O_3 and $Mg(OH)_2$ + RE_2O_3 from inside to outside. The inner RE_2O_3 layer and MgO + RE_2O_3 layer play an important role in the formation of the film. The compact inner film can prevent the corrosion medium from reacting with Mg matrix. Rare earth oxides may have two formation modes. Rare earth elements (Y, Gd, Nd) generate RE^{3+} ions through anodic reaction, and then react with oxygen and hydrogen in the film to generate $RE(OH)_3$. The $RE(OH)_3$ with unstable chemical properties is easy to dehydrate to form stable RE_2O_3 [12]. Another reaction might be $2RE+3H_2O\rightarrow RE_2O_3+3H_2$, that is, rare earth elements react with penetrating water molecules. Rare earth oxides grow coherently along the (002) plane of MgO (Fig. 4(b)), fill the gap of MgO and form a dense film with PBR value of 1.1653, which can provide good protection.

5 Conclusions

(1) The inward oxidation process of Mg and the external oxidation process of rare earth elements coexist in the corrosion process of aged WE43 alloy. The precipitates are preferentially oxidized and participate in the formation process of the corrosion film.

(2) The dense corrosion product film formed on aged WE43 alloy is a three-layer structure, which is RE_2O_3, MgO layer doped with RE_2O_3 and $Mg(OH)_2$ layer doped with RE_2O_3 from inside to outside. The PBR rate of RE_2O_3 layer is calculated to be 1.1653. The inner RE_2O_3 layer and MgO layer doped with RE_2O_3 play an important role in the formation of the film.

(3) Rare earth oxides have the preferential relationship $(\bar{2}11)//(002)_{MgO}$ and $[231]//[\bar{1}\bar{1}0]_{MgO}$ with MgO. The oxide particles can fill the gap of porous MgO layer, which improves the compactness of the film and make film good protection.

CRediT authorship contribution statement

Yong CAI: Writing – Original draft, Writing – Review & editing, Validation, Data curation, Investigation; **Yi-peng CHEN:** Writing – Review & editing, Formal analysis, Data curation; **Hong YAN:** Writing – Review & editing, Validation; **Rong-shi CHEN:** Writing – Review & editing, Validation, Supervision, Resources, Project administration, Funding acquisition, Conceptualization.

Declaration of competing interest

The authors declare that they have no known competing financial interests or personal relationships that could have appeared to influence the work reported in this paper.

Acknowledgments

This work was financially supported by the National Natural Science Foundation of China (No. 52271107), the Natural Science Foundation of Liaoning Province, China (No. 2020-MS-004), and the Natural Science Foundation of Shandong Province, China (No. ZR2021ME241).

References

[1] JIANG Bin, DONG Zhi-hua, ZHANG Ang, SONG Jiang-feng, PAN Fu-sheng. Recent advances in micro-alloyed

wrought magnesium alloys: Theory and design [J]. Transactions of Nonferrous Metals Society of China, 2022, 32: 1741−1780.

[2] SONG Jiang-feng, CHEN Jing, XIONG Xiao-ming, PENG Xiao-dong, CHEN Dao-lun, PAN Fu-sheng. Research advances of magnesium and magnesium alloys worldwide in 2021 [J]. Journal of Magnesium and Alloys, 2022, 10: 863−898.

[3] SHIRI M, JAFARI H, SINGH R. Effect of extrusion parameters on degradation of magnesium alloys for bioimplant applications: A review [J]. Transactions of Nonferrous Metals Society of China, 2022, 32: 2787−2813.

[4] GOGHERI M S, KASIRI-ASGARANI M, BAKHSHESHI-RAD H R, GHAYOUR H, RAFIEI M. Mechanical properties, corrosion behavior and biocompatibility of orthopedic pure titanium−magnesium alloy screw prepared by friction welding [J]. Transactions of Nonferrous Metals Society of China, 2020, 30: 2952−2966.

[5] CHU P W, MARQUIS E A. Linking the microstructure of a heat-treated WE43 Mg alloy with its corrosion behavior [J]. Corrosion Science, 2015, 101: 94−104.

[6] ZUCCHI F, GRASSI V, FRIGNANI A, MONTICELLI C, TRABANELLI G. Electrochemical behaviour of a magnesium alloy containing rare earth elements [J]. Journal of Applied Electrochemistry, 2006, 36: 195−204.

[7] YAO H B, LI Y, WEE A T S. An XPS investigation of the oxidation/corrosion of melt-spun Mg [J]. Applied Surface Science, 2000, 158: 112−119.

[8] SANTAMARIA M, DI QUARTO F, ZANNA S, MARCUS P. Initial surface film on magnesium metal: A characterization by X-ray photoelectron spectroscopy (XPS) and photocurrent spectroscopy (PCS) [J]. Electrochimica Acta, 2007, 53: 1314−1324.

[9] LIU M, ZANNA S, ARDELEAN H, FRATEUR I, SCHMUTZ P, SONG G L, ATRENS A, MARCUS P. A first quantitative XPS study of the surface films formed, by exposure to water, on Mg and on the Mg−Al intermetallics: Al_3Mg_2 and $Mg_{17}Al_{12}$ [J]. Corrosion Science, 2009, 51: 1115−1127.

[10] TAHERI M, PHILLIPS R C, KISH J R, BOTTON G A. Analysis of the surface film formed on Mg by exposure to water using a FIB cross-section and STEM−EDS [J]. Corrosion Science, 2012, 59: 222−228.

[11] BRADY M P, ROTHER G, ANOVITZ L M, LITTRELL K C, UNOCIC K A, ELSENTRIECY H H, SONG G L, THOMSON J K, GALLEGO N C, DAVIS B. Film breakdown and nano-porous $Mg(OH)_2$ formation from corrosion of magnesium alloys in salt solutions [J]. Journal of the Electrochemical Society, 2015, 162: 140−149.

[12] ARDELEAN H, SEYEUX A, ZANNA S, PRIMA F, FRATEUR I, MARCUS P. Corrosion processes of Mg−Y−Nd−Zr alloys in Na_2SO_4 electrolyte [J]. Corrosion Science, 2013, 73: 196−207.

[13] UNOCIC K A, ELSENTRIECY H H, BRADY M P, MEYER H M, SONG G L, FAYEK M, MEISNER R A, DAVIS B. Transmission electron microscopy study of aqueous film formation and evolution on magnesium alloys [J]. Journal of the Electrochemical Society, 2014, 161: 302−311.

[14] PHILLIPS R C, KISH J R. Nature of surface film on matrix phase of Mg alloy AZ80 formed in water [J]. Corrosion, 2013, 69: 813−820.

[15] LIU M, SCHMUTZ P, UGGOWITZER P J, SONG G L, ATRENS A. The influence of yttrium (Y) on the corrosion of Mg−Y binary alloys [J]. Corrosion Science, 2010, 52: 3687−3701.

[16] MORDIKE B L. Creep-resistant magnesium alloys [J]. Materials Science and Engineering: A, 2002, 324: 103−112.

[17] KANG Y H, WANG X X, ZHANG N, YAN H, CHEN R S. Effect of initial temper on the creep behavior of precipitation-hardened WE43 alloy [J]. Materials Science and Engineering: A, 2017, 689: 419−426.

[18] KHARITONOV D S, ZIMOWSKA M, RYL J, ZIELIŃSKI A, OSIPENKO M A, ADAMIEC J, WRZESIŃSKA A, CLAESSON P M, KURILO I I. Aqueous molybdate provides effective corrosion inhibition of WE43 magnesium alloy in sodium chloride solutions [J]. Corrosion Science, 2021, 190: 109664.

[19] SUN Wan-ting, WU Bo, FU Hui, YANG Xu-sheng, QIAO Xiao-guang, ZHENG Ming-yi, HE Yang, LU Jian, SHI San-qiang. Combining gradient structure and supersaturated solid solution to achieve superior mechanical properties in WE43 magnesium alloy [J]. Journal of Materials Science & Technology, 2022, 99: 223−238.

[20] PEREIRA G S, KOGA G Y, AVILA J A, BITTENCOURT I M, FERNANDEZ F, MIYAZAKI M H, BOTTA W J, BOSE F W W. Corrosion resistance of WE43 Mg alloy in sodium chloride solution [J]. Materials Chemistry and Physics, 2021, 272: 124930.

[21] PRZONDZIONO J, WALKE W, HADASIK E, SZALA J, WIECZOREK J. Corrosion resistance tests of magnesium alloy WE43 after extrusion [J]. Metalurgija, 2013, 52: 243−246.

[22] FENG Bao-jing, LIU Guo-nan, YANG Pei-xu, HUANG Sen-sen, QI Dong-qing, CHEN Peng, WANG Cheng-duo, DU Jiang, ZHANG Shao-jun, LIU Jin-hui. Different role of second phase in the micro-galvanic corrosion of WE43 Mg alloy in NaCl and Na_2SO_4 solution [J]. Journal of Magnesium and Alloys, 2022, 10: 1598−1608.

[23] KANG Yue-hua, YAN Hong, CHEN Rong-shi. Effects of heat treatment on the precipitates and mechanical properties of sand-cast Mg−4Y−2.3Nd−1Gd−0.6Zr magnesium alloy [J]. Materials Science and Engineering: A, 2015, 645: 361−368.

[24] SONG Guang-ling, UNOCIC K A. The anodic surface film and hydrogen evolution on Mg [J]. Corrosion Science, 2015, 98: 758−765.

[25] BRADY M P, FAYEK M, ELSENTRIECY H H, UNOCIC K A, ANOVITZ L M, KEISER J R, SONG G L, DAVIS B. Tracer film growth study of hydrogen and oxygen from the corrosion of magnesium in water [J]. Journal of the Electrochemical Society, 2014, 161: 395−404.

[26] CZERWINSKI F. The oxidation behaviour of an AZ91D magnesium alloy at high temperatures [J]. Acta Materialia, 2002, 50: 2639−2654.
[27] JIANG Quan-tong, LU Dong-zhu, LIU Chang, LIU Na-zhen, HOU Bao-rong. The Pilling−Bedworth ratio of oxides formed from the precipitated phases in magnesium alloys [J]. Frontiers in Materials, 2021, 8: 1−12.
[28] XU Chun-hua, GAO Wei. Pilling−Bedworth ratio for oxidation of alloys [J]. Material Research Innovations, 2000, 3: 231−235.

时效态 WE43 合金表面腐蚀产物膜的显微组织

蔡 勇[1,2]，陈翌鹏[1,2]，闫 宏[2,3]，陈荣石[2]

1. 中国科学技术大学 材料科学与工程学院，沈阳 110016；
2. 中国科学院金属研究所 师昌绪先进材料创新中心，沈阳 110016；
3. 山东科技大学 材料科学与工程学院，青岛 266590

摘 要：时效态 WE43 合金在 3.5 wt.% NaCl 溶液中形成了致密且具有 3 层结构的腐蚀产物膜。采用透射电子显微镜分析膜层的显微组织。保护性膜层为 3 层结构，从内到外依次为 RE_2O_3 层、MgO 与 RE_2O_3 的混合层和 $Mg(OH)_2$ 与 RE_2O_3 的混合层。析出相和稀土元素通过外氧化的方式形成大量稀土氧化物颗粒，这是保护性膜层形成的主要原因。RE_2O_3 与 MgO 存在以下择优位向关系：$(\bar{2}11)$晶面和[231]晶向分别与 MgO 的(002)晶面和[110]晶向平行。因此，稀土氧化物颗粒可以填补疏松 MgO 膜层的空隙，从而提高了膜层的致密性。内层的 RE_2O_3 和 MgO 与 RE_2O_3 的混合层对于保护性膜层的形成起到了重要作用。致密的内层腐蚀产物膜能阻止腐蚀介质与镁基体发生反应。

关键词：镁合金；腐蚀产物膜；高分辨透射电镜；析出相；氧化

(Edited by Wei-ping CHEN)